Available on CMS information server

CMS NOTE 2005/018

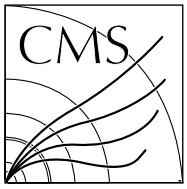

The Compact Muon Solenoid Experiment

CMS Note

Mailing address: CMS CERN, CH-1211 GENEVA 23, Switzerland

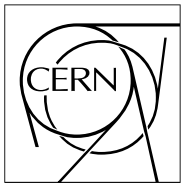

October 4, 2005

Parametrization of the Response of the Muon Barrel Drift Tubes

J. Puerta-Pelayo[a], M.C. Fouz, P. Garcia-Abia

Particle Physics Division, CIEMAT, Madrid (Spain)

Abstract

This note describes the parametrization of the response of the drift cells of the CMS barrel muon chambers based on the final design of the cell. The details of the simulation of the cell with the GARFIELD program are presented, together with comparisons with test beam data. The results, expressed in terms of the time-to-drift-distance relation of the cell for different configurations of the magnetic field and for different incidence angle of particles, are contained in a set of digitization functions which have become part of the official simulation and reconstruction software of CMS. This function supersedes previous results based on earlier designs of the drift tubes.

[a] Now at CERN, Geneva (Switzerland).

1 Introduction

The drift tube chambers used for muon tracking in the central region of CMS ($|\eta| < 1.2$) are composed of several layers of staggered rectangular drift cells [1, 2]. Each cell consists of a central sense wire, cathodes at both ends of the cell and shaping electrodes, operating in an Ar/CO_2 environment.

The design of the drift cell has undergone several modifications and improvements since the first stages of the experiment. The cell dimensions and the layout of the cathode in the final design are significantly different from those described in the Technical Design Report [1] and for which a parametrization of the cell response versus the magnetic field [3] based on a detailed simulation already exists [4].

This note describes the parametrization of the response of the drift cells using the final design parameters. The simulation was done using GARFIELD [5], a standard program for the simulation of gaseous detectors. Based on previous experience, our main objective was to parametrize the response of the cell for different configurations of the magnetic field and incidence angle of muons. The parametrization has been implemented as a set of functions that provide the expected drift time for any muon position along the cell (for use in signal simulation), as well as the position along the cell for a given drift time (for use in reconstruction). These functions are included in the current official CMS simulation software, OSCAR [6], and reconstruction software, ORCA [7].

2 Simulation with GARFIELD

GARFIELD is a software package designed for the detailed simulation of wire chambers in two and three dimensions. Starting from the geometrical definition of the cell, the electrostatic configuration and the existing magnetic field, GARFIELD reproduces the drift behaviour of the ionizing particles taking into account diffusion, avalanche development and signal induction. Moreover, it calculates the properties of any gas mixture such as drift velocity, Townsend coefficient, cluster size, etc., using specific programs like HEED [8] and MAGBOLTZ [9].

2.1 Cell definition

The first step of the simulation is the geometrical definition of the cell: its two-dimensional section is introduced as a transverse section of the actual cell, although the third coordinate is considered as well.

GARFIELD was conceived for the simulation of multi-wire chambers and therefore does not deal with finite surfaces. Despite this, the simulation of the whole cell can be done by describing the electrodes and other electrostatic surfaces as continuous rows of infinite length wires with specific voltages and cross-sections. The strips and cathodes are defined with voltages 1800 V and -1200 V, respectively, while the cell volume is enclosed by a series of grounded wires simulating the plates and the I-beams. The sense wire is placed in the center of the cell with an operating voltage of 3600 V. We refer to the volume enclosed by the wires as the "sensitive volume". GARFIELD calculates the global electrostatic configuration of the cell and the electric field at each point of the active area defined by the sensitive volume. Figure 1 depicts the schematic of the cell used in the simulation, which matches the dimensions of the final hardware design.

The number of wires "per surface" can be chosen. A large number of wires per row provides a better approximation of a surface, at the expense of increasing the computing time required for processing the cell configuration. The wire density used, 5 wires/mm, achieves an adequate compromise between both factors.

It must be pointed out that the cell dielectrics (Mylar tapes) have not been included in the simulation. GARFIELD is able to consider the simulation of dielectric materials in only a few configurations. However, previous studies of the effect of dielectrics in the cell, using the program POISSON [10], have shown the influence on the global electrostatic configuration of the cell to be almost negligible. Therefore their inclusion in the simulation is not expected to substantially modify the results [11].

2.2 Gas

The second step of the simulation is the specification of the gas. Parameters like pressure, temperature and the magnetic field in which the cell is embedded, are taken into account in the simulation since they affect the drift properties of the gas.

In order to calculate the transport properties of ions and electrons the correct gas mixture, 85% Ar / 15% CO_2 by volume, was introduced by means of the HEED program. This program simulates the ionization energy loss

of traversing particles in the gas volume. Figure 2 shows the predicted energy loss for muons, as a function of the muon energy. HEED also calculates the number of primary and secondary electrons generated, the diffusion coefficients and the cluster size (Figure 3). Other physical processes like Auger electrons, photon emission and delta rays, are also simulated.

2.3 Drift

Once all the features of the cell are defined, its electrostatic configuration and drift properties are determined. Starting from them it is possible to simulate the behaviour of the cell as a detector. Figure 4 displays the values of the electric potential throughout the cell. The field outside the sensitive volume is not considered. The predicted electron drift velocity is also shown for different values of the electric field. It can be seen from this graph that, for the nominal electric field ($\sim$ 1.9 kV/cm), the drift velocity is stable around 55 $\mu\mathrm{m}/\mathrm{ns}$, in agreement with experimental measurements of a real drift cell [12].

For a more detailed study of drift processes, we simulated muons traversing the cell. Given a particle track in the sensitive volume, GARFIELD is able to simulate the production of ionization electrons and the other physical processes involved. The drift of each electron toward the anode wire is simulated and the relevant information like drift trajectories, number of electrons reaching the wire, multiplication processes, drift times, etc., is recorded. For each trajectory, the arrival times of each primary ionization electron is calculated, as well as its origin, emission angle, etc.

The maximum drift time of the cell can be obtained from the drift time measured in cells of three consecutive layers (t_1, t_2 and t_3) of the same chamber. The *mean-timer*, defined as $MT = (t_1 + t_3)/2 + t_2$, gives an experimental determination of the maximum drift time, and is useful for the comparison of the simulation and the experimental data.

Figure 5 shows the drift trajectories of the ionization electrons generated by a 100 GeV muon crossing the cell, with and without magnetic field. The upper-left figure is without magnetic field and also shows a delta ray emitted toward the wire, together with its associated secondary ionization, which will induce drift times significantly lower than those of the primary electrons. The upper-right plot, with magnetic field on, shows the asymmetries in the drift trajectories caused by the field.

2.4 Treatment of Delta Rays

HEED simulates the ejection of electrons from atoms due to the incident charged particle. Electrons with sufficient energy may cause further ionization (giving rise to delta rays), otherwise they are drifted through the detector gas. The emission of Auger electrons and fluorescence photons from the excited atoms are also considered. HEED does not create clusters, treating each delta electron as an individual cluster of size 1.

3 Parametrization

The parametrization of the cell response must be implemented in the CMS software as a set of functions capable of providing the expected drift time, given a certain muon trajectory, in any magnetic field configuration. In order to achieve this, traversing muons were simulated homogeneously in 0.2 mm steps along the x-axis. In each of these steps 500 muons of 100 GeV were simulated for an atmospheric pressure of 1 atm and 25°C temperature. The arrival times and origin points of the 5^{th} to 8^{th} primary electrons were recorded.

The drift trajectories depend on the magnetic field configuration and incidence angle of the muons, giving rise to different arrival time distributions. In order to cover all the configurations expected in CMS, a grid of values of the radial, B_y, and longitudinal, B_z, components of the magnetic field and of the incidence angle of the muons was defined:

B_y (T)	B_z (T)	Angle (degrees)
0	0	0
0.1	0.05	$\pm$ 5
0.2	0.1	$\pm$ 10
0.35	0.2	$\pm$ 15
0.75	0.4	$\pm$ 30
		$\pm$ 45

The simulation of the entire cell was then repeated for each of the 275 possible combinations of these values. Due to the asymmetry induced in the cell by the magnetic field (Figure 5) it was necessary to simulate both positive and negative angles. In the presence of magnetic fields parallel to the wire, the drift trajectories of muons with positive and negative angles are different, hence the combined effect of angle and B_z induces an asymmetric behaviour which must be considered.

As an example, Figure 6 (left) shows the arrival time distributions obtained for the $5^{\rm th}$ electron from 500 simulated tracks with a 30 degree angle at 1.92 cm from the wire. The plot on the right displays the arrival times for all the primary electron superimposed.

It is necessary to choose a specific electron as the trigger electron, in order to use its arrival time for the parametrization. Due to the expected gain in the wire region, a single electron can induce the charge required to reach the discrimination threshold of the electronics. However, the avalanche has a time development which may allow further electrons to reach the wire and to initiate avalanches which also contribute to the integrated charge before it reaches the discriminator threshold. To select which electron to use, a comparison with the experimental data was made.

Figure 7 (left) shows the arrival time distribution of the $5^{\rm th}$ electron for all tracks simulated along the cell in a standard configuration (no B field, normal incidence). The same distribution obtained with real muons in a test beam [12] is superimposed. For this comparison, events containing delta rays arising from the aluminium plates, energetic enough to mask a real signal in the cell (which we refer to as "hard delta rays"), were rejected from the experimental data by applying cuts in the mean-timers [13]. Note that this effect is not considered in GARFIELD. The agreement between the distributions of Figure 7 (left) is very good.

For the same subset of real events (no hard delta rays) a comparison of mean-timer distributions was carried out. For the simulated data, the mean-timers were calculated by combining arrival times coming from different positions along the cell. These are displayed in Figure 7 (right) for the $5^{\rm th}$, $6^{\rm th}$ and $7^{\rm th}$ electron. Clearly, the fifth electron reproduces well the behaviour of the real data, in terms both of measured times and width of the distribution. Finally, Figure 8 plots the values of the drift velocity calculated from the arrival time of the $5^{\rm th}$ electron, as functions of the components of the magnetic field and the incidence angle. The results obtained from test beam data [12] are also displayed, showing very good agreement with the simulation.

Driven by these considerations, we define the fifth electron reaching the wire as the effective trigger electron. We assume that at that moment the integrated charge induced by avalanches of preceding electrons reaches the threshold of the electronics, corresponding to 15 mV. Under this assumption, we used as estimator of the average drift time at each position the arrival time distributions analogous to those of Figure 6. These distributions are asymmetric with a width due to diffusion, non-linearities and delta rays. The average value is obtained from an asymmetric Gaussian fit with independent widths at each side of the maximum, as indicated in Figure 6. The average values, maximum of the distribution and both widths are recorded.

The distribution of the central values versus the position along the cell is shown in Figure 9 for two configurations. The slope of these distributions is used as the estimator of the drift velocity in each configuration. For this purpose, a linear fit is performed in the central part of the cell (from 2.5 mm to 19 mm from the wire) which is, as we will see later, less influenced by non-linearities originating from the magnetic field and incidence angle.

Once the drift time has been estimated, a deviation from the linear space-time relationship can be calculated:

$$\Delta t = t_{sim} - \left(\frac{x}{v_d} + b \right) \tag{1}$$

where v_d and b are the parameters of the linear fit and t_{sim} is the peak value of the drift time distribution at that position. The distribution $\Delta t(x)$ is what we call *deviation from linearity* at a given position. This deviation affects mainly the wire and cathode regions. The magnetic field in the z direction and the incidence angle induce a degradation of the linear behaviour of the cell, as can be seen in Figure 10 for B_y = 0.75 T, B_z = 0.40 T and 30 degrees. B_y essentially does not affect the linearity.

For each configuration of angle and magnetic field, a polynomial fit is performed to the distribution of linearity deviations. The fit is made for the values of $\Delta t(x)$, the widths on each side of the peak ($\sigma_p(x)$ towards greater drift times, and $\sigma_m(x)$ towards lower times) and the inverse function $\Delta x(t)$, which provides linearity deviations in position for a given drift time. Figure 11 shows two examples of these fits for the case B_y = 0.75 T, B_z = 0.40 T and 30 degrees, for both $\Delta t(x)$ and $\Delta x(t)$. The first example was adjusted to polynomial branches in four different regions, whereas for the second only three branches were used. The fits of the widths $\sigma_p(x)$ and $\sigma_m(x)$ were made in a similar way.

4 Digitization

Once the complete set of parametrization functions in all simulated configurations had been obtained, they were implemented in a C++ program, which is now part of the official reconstruction and simulation software of the CMS experiment. The code and a README with the description of the technical details can be found here:

http://wwwae.ciemat.es/∼pablog/cms/MB_DriftTime_V2.1.tgz

http://wwwae.ciemat.es/∼pablog/cms/README_V2.1

The program contains two functions. Function MB_DT_drift_time() of class MuBarDriftTimeParametrization provides the drift time, the linearity deviation and the widths σ_p and σ_m at any position along the cell, for a given configuration of incidence angle and magnetic field. Function MB_DT_drift_distance() of class MuBarTime2DriftParametrization performs the inverse operation, returning the drift distance and its uncertainty, given a drift time in a certain $\vec{B}$ and angle configuration.

The first function performs a simple operation: given a position of the muon along the cell and a configuration of the magnetic field, it takes the nearest simulated points in the three-dimensional grid (angle, B_y, B_z) and performs a multidimensional linear interpolation of the parametrization in those points. The interpolation is carried out for the parametrization of Δt, the drift velocity and both widths. Once these values have been calculated, the drift time is obtained through:

$$t_d = \left(\frac{x}{v_d} + b\right) + \Delta t \tag{2}$$

The inverse function follows a similar procedure, extracting the drift distance as:

$$x = (v_d \cdot t_d + b) + \Delta x \tag{3}$$

Both functions can be invoked with the interpolation inhibited, and they then provide as output the parametrization for the nearest point in the grid (B_y, B_z, angle). The slightly lower accuracy in this case is compensated by a reduced processing time.

Figure 12 (left) shows several Δt values provided by the function in some configurations. The 20 degree values are examples of interpolated values, which have not been directly simulated, and hence confirm the reasonable behaviour of the interpolation. The difference between the input and the reconstructed position is shown in Figure 12 (right). The intrinsic fluctuations of the function and the effect of the widths cause discrepancies in some cases, although these deviations remain below 50 μm in almost all configurations.

5 Conclusions

We have described the results of the simulation and the parametrization of the drift cell of the barrel muon drift tubes of CMS. The time response of the detector is well-modeled by the GARFIELD prediction of the distribution of arrival times at the wire of the fifth primary electron. It has been shown that this choice provides excellent agreement with the experimental data.

Using these drift time distributions, the behaviour of the drift cell has been parametrized over a wide range of values of the applied magnetic field and the incidence angles of traversing muons. The parametrization of the cell response has been implemented in a C++ code which is currently used in the official simulation and reconstruction software of CMS.

6 Acknowledgments

We thank our colleagues from the PRS muon group for their advice and fruitful discussions, in particular Richard Breedon and Timothy Cox for the careful reading of the manuscript. We greatly appreciate the help of Nicola Amapane with the implementation of the digitization code in the simulation and reconstruction software of CMS.

References

[1] *"The CMS muon project, CMS Technical Design Report"*, CERN/LHCC 97-32, CMS TDR, December 1997.

[2] M. Benettoni *et al.* , Nucl. Instr. and. Met. A 410 (1998), 133;
M. Aguilar-Benitez *et al.* , Nucl. Instr. and. Met. A 416 (1998), 243;
S. Bethke *et al.* , CMS Note 1998/064.

[3] A. Gresele and T. Rovelli, *"Parameterization of B Field Effects in DTBx"*, CMS Note 1999/064, September 1999.

[4] T. Rovelli, *"Simulation of the CMS Barrel Muon Chambers"*, CMS-TN/95-106, June 1995;
T. Rovelli and V. Tano, *"Detailed simulation of Drift Tubes"*, Nuclear Physics B, 54B (1997) 323.

[5] R. Veenhof, *"GARFIELD. Simulation of gaseous detectors"*, CERN Writeups, Ref. W5050,
`http://consult.cern.ch/writeup/garfield/`.

[6] *"Object-oriented Simulation for CMS Analysis and Reconstruction"*,
`http://cmsdoc.cern.ch/oscar/`.

[7] *"Object-oriented Reconstruction for CMS Analysis"*,
`http://cmsdoc.cern.ch/orca/`.

[8] I. Smirnov, *"HEED. Interactions of particles with gases"*, CERN Writeups, Ref. W5060,
`http://consult.cern.ch/writeup/heed/`.

[9] S. Biagi, *"Magboltz: Transport of electrons in gas mixtures"*, CERN Writeups,
`http://consult.cern.ch/writeup/magboltz/`.

[10] M. Guijarro, *"Poisson: Reference manual"*, CERN Writeups,
`http://consult.cern.ch/writeup/poisson/`.

[11] H. Schwarthoff, *"Simulationen in Konzeption und Bau der zentralen Myondriftkammern am CMS-Detektor"*, Ph.D. Thesis, RWTH Aachen, 1997.

[12] M.Aguilar-Benítez *et al.*, *"Test Beam Results Obtained with the Q4 Prototype"*, Nucl. Instr. and. Met. A 480 (2002), 658;
M. Cerrada *et al.*, *"Results from the Analysis of the Test Beam Data taken with the Barrel Muon DT Prototype Q4"*, CMS Note 2001/041, April 2001.

[13] J. Puerta-Pelayo, *"Estudio sobre las cámaras de tubos de deriva para el espectrómetro de muones del experimento CMS"*, Ph.D. Thesis, Universidad Autónoma de Madrid, April 2004; CMS THESIS 2004-008.

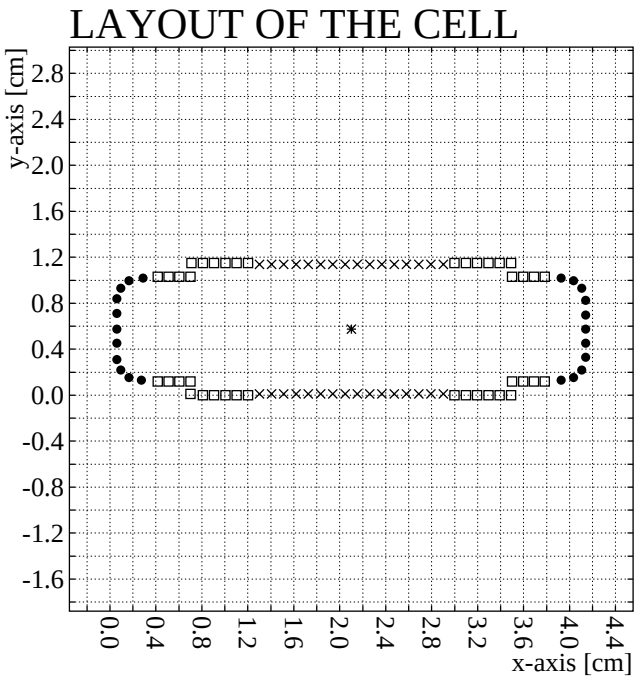

Figure 1: Layout of the simulated cell. Different symbols represent different voltages: cathodes (dot), shaper strips (cross), sense wire (asterisk) and ground (square). The number of wires used in the simulation is five times greater than that displayed in the graph.

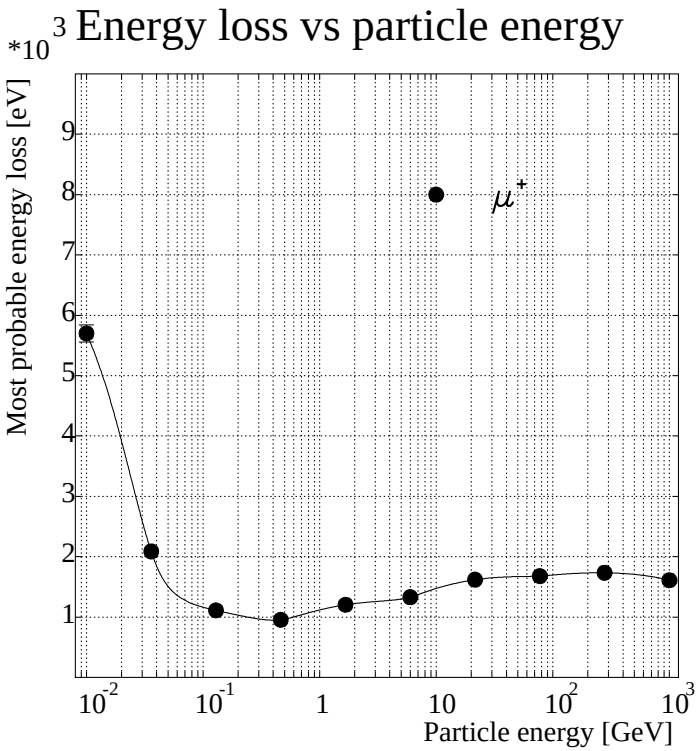

Figure 2: Most probable value of the ionization energy loss versus muon energy, for muons crossing the simulated cell, calculated with the HEED program.

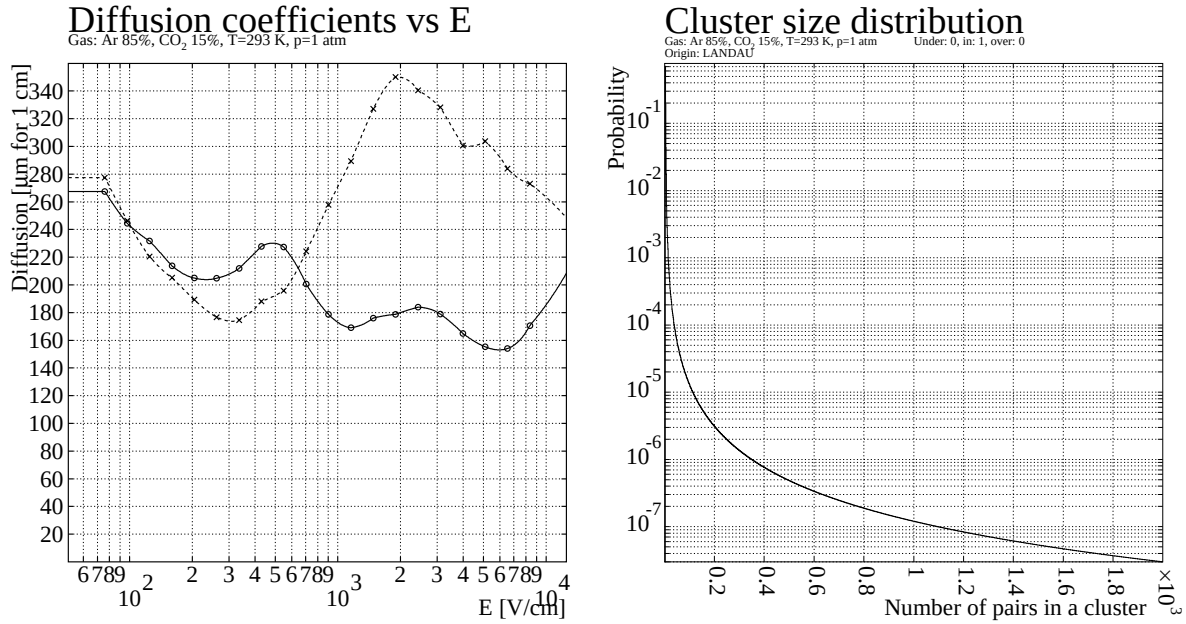

Figure 3: (Left) Transverse (dashed) and longitudinal (solid) diffusion coefficients versus electric field, calculated by HEED in the absence of magnetic field. (Right) Cluster size distribution for the simulated cell.

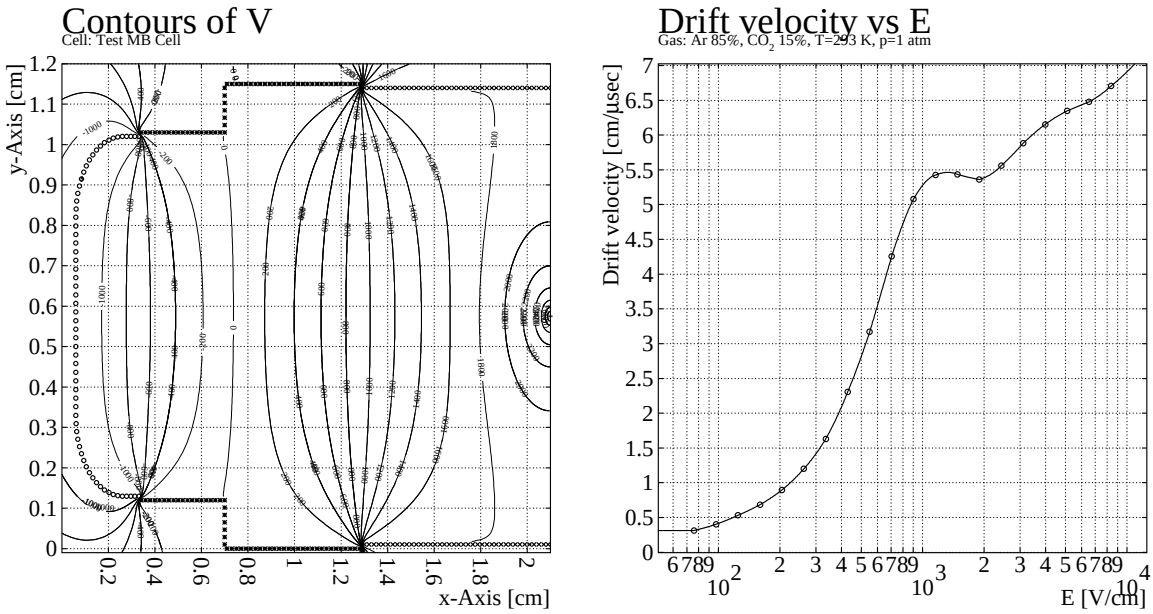

Figure 4: (Left) Equipotential lines computed by GARFIELD for a half-cell. (Right) Drift velocity of electrons as function of the electric field along the cell.

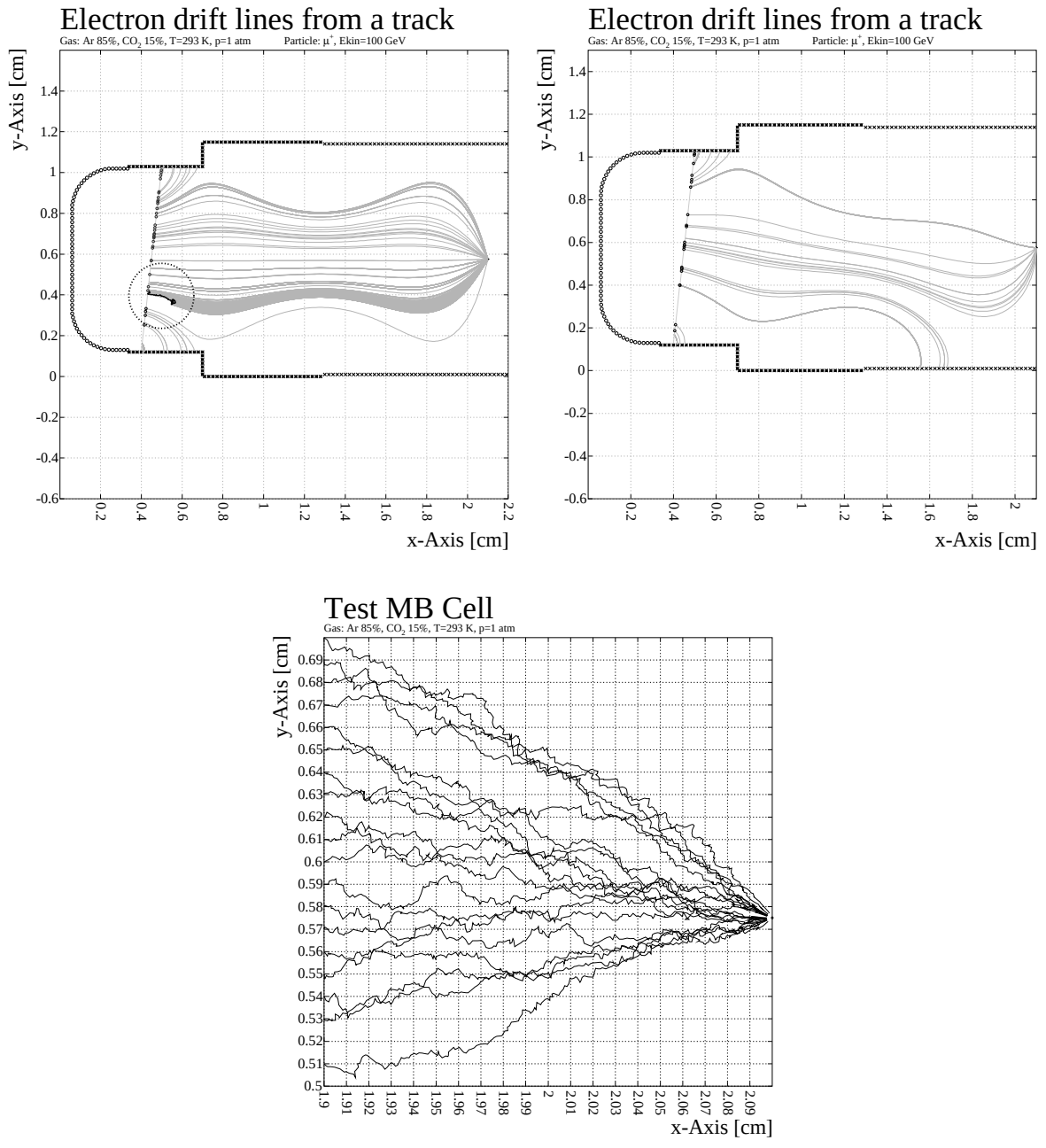

Figure 5: Drift trajectories corresponding to primary ionizing electrons caused by a 100 GeV muon crossing the simulated cell. (Upper left) A muon traversing the cell with a certain angle. The trajectory of an energetic delta ray can be seen inside the dotted circle. This delta ray produces secondary ionizations far from the point of origin giving rise to drift times earlier than the other primary electrons. (Upper right) The same situation in the presence of a 0.4 T magnetic field parallel to the wire. The curvature in the drift trajectories can be seen, as well as the asymmetry induced in the cell by this field. (Lower) Expanded view of the region of the wire in the absence of magnetic field.

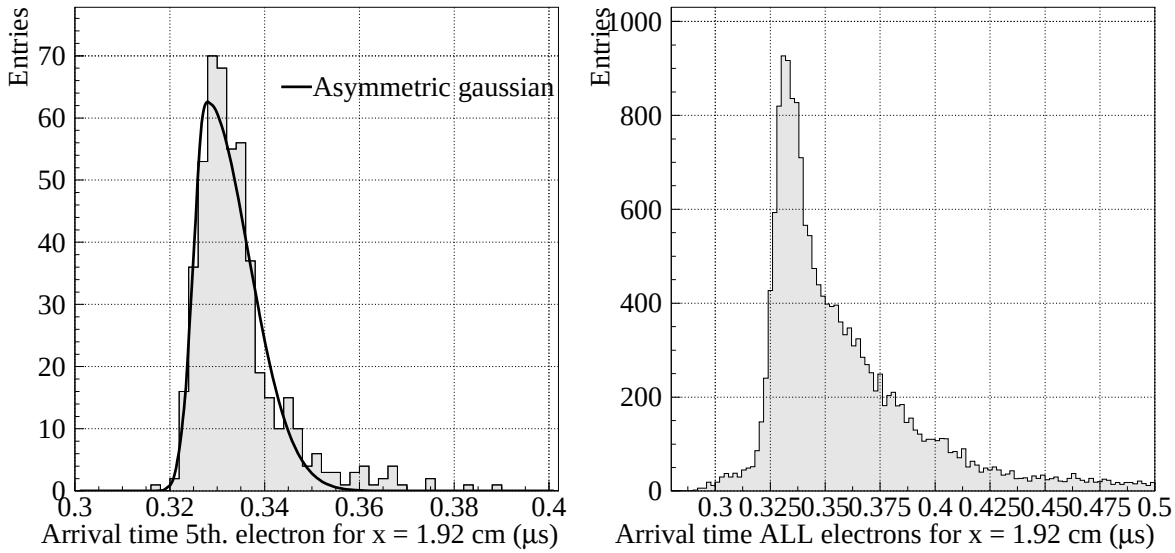

Figure 6: (Left) Arrival time distribution from a sample of 500 muons crossing the cell at an angle of 30 degrees, at a distance 1.92 cm from the wire and in a magnetic field of B_z = 0.4 T. The line shows the result of an asymmetric Gaussian fit. (Right) Arrival times of all the electrons reaching the wire, in the same configuration.

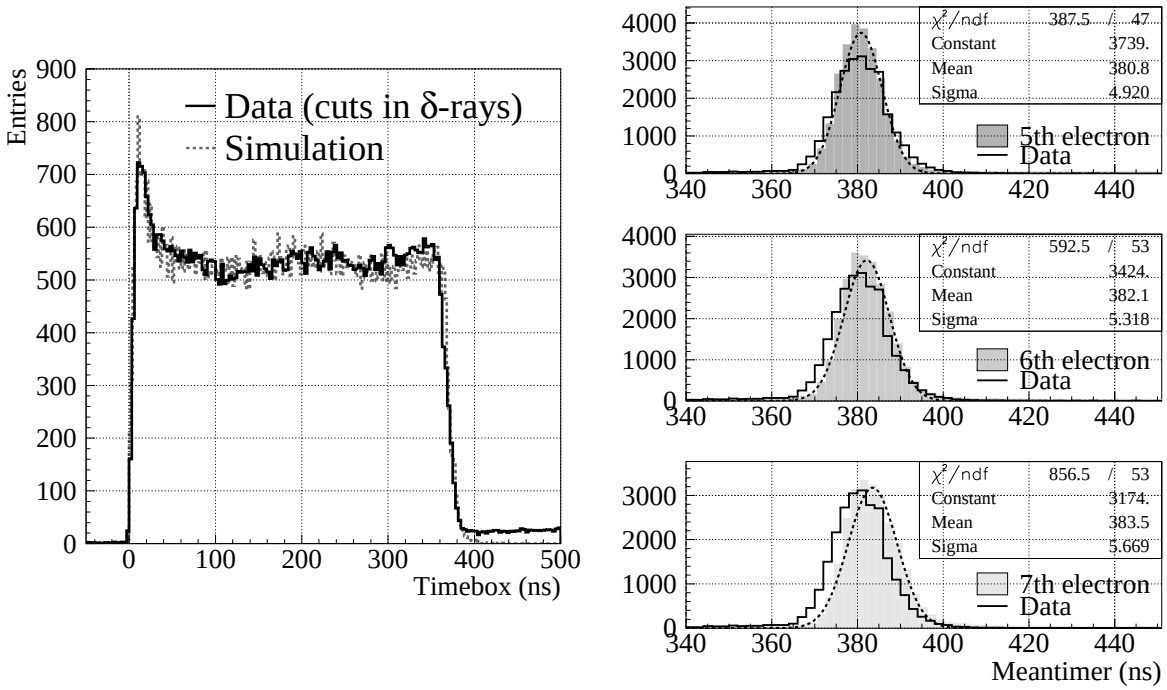

Figure 7: (Left) Drift time distribution predicted by the simulation (dashed line) and in reality (solid line), after subtracting events with hard delta rays arising from the aluminium plates. The agreement is good. (Right) Simulated mean-timer distributions obtained from the arrival times of the $5^{\rm th}$, $6^{\rm th}$ and $7^{\rm th}$ electrons, together with the result of Gaussian fits these distributions (dashed lines). The experimental distributions are also shown. The best agreement is obtained for the $5^{\rm th}$ electron.

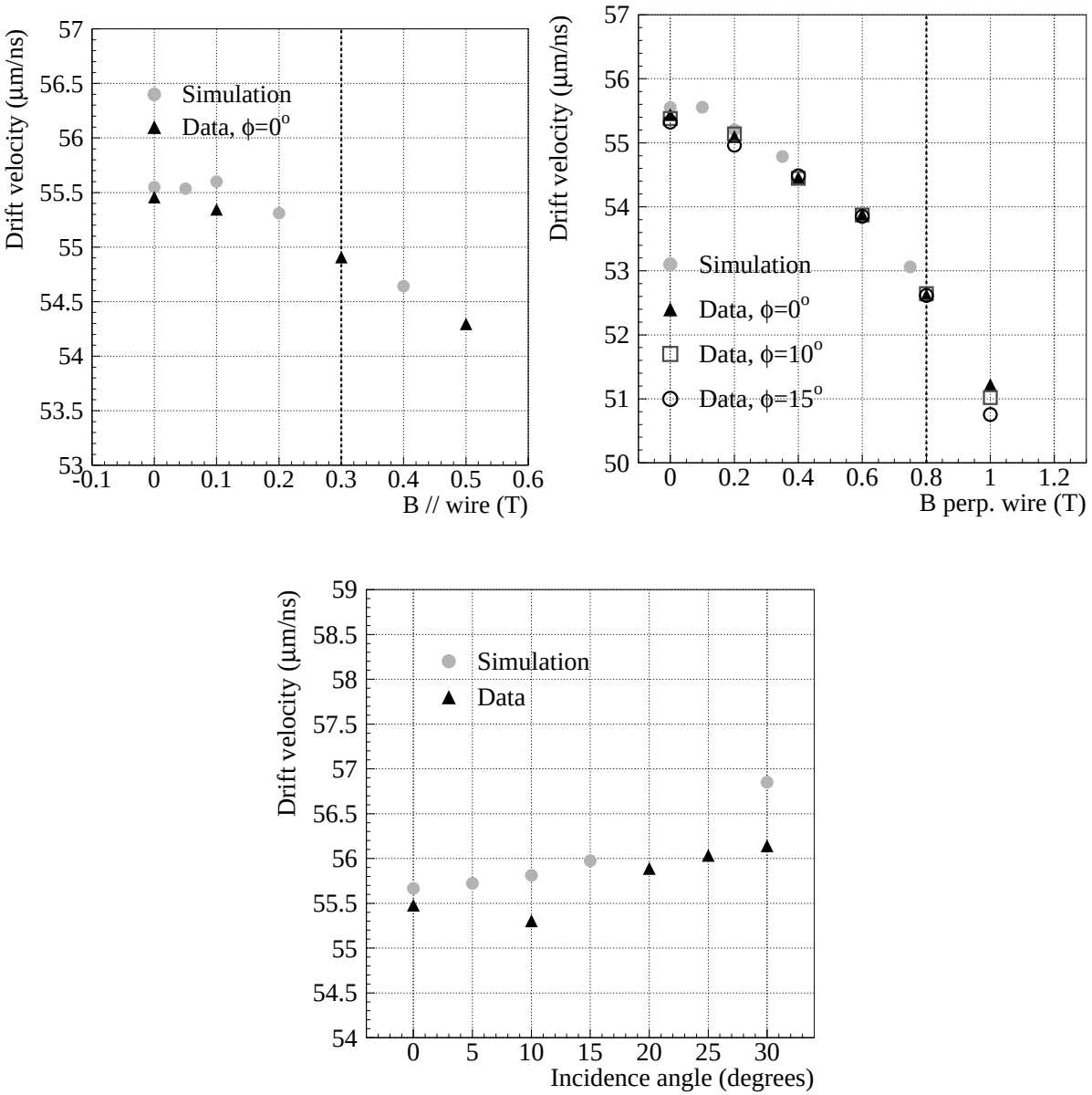

Figure 8: Drift velocities calculated with the arrival times of the 5^{th} electron compared to the experimental values. The comparison is done for the magnetic fields and angles used in our simulation.

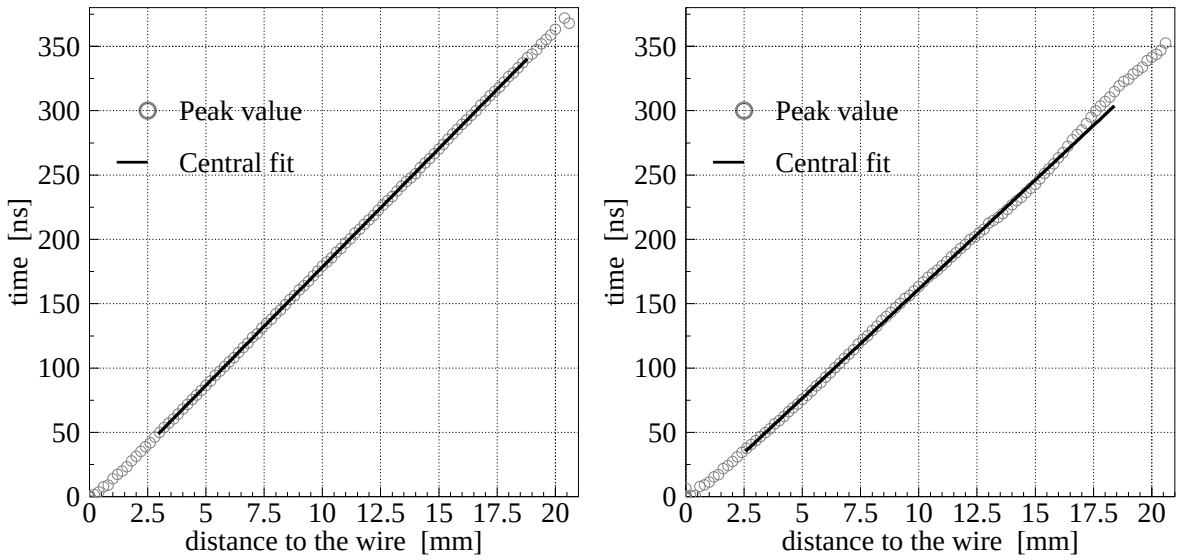

Figure 9: Estimated drift time versus distance to the wire. The slope of the distributions provides an estimator of the drift velocity. The left plot corresponds to normal incidence, whereas the right plot was obtained with a configuration of B_z = 0.4 T and 30 degrees.

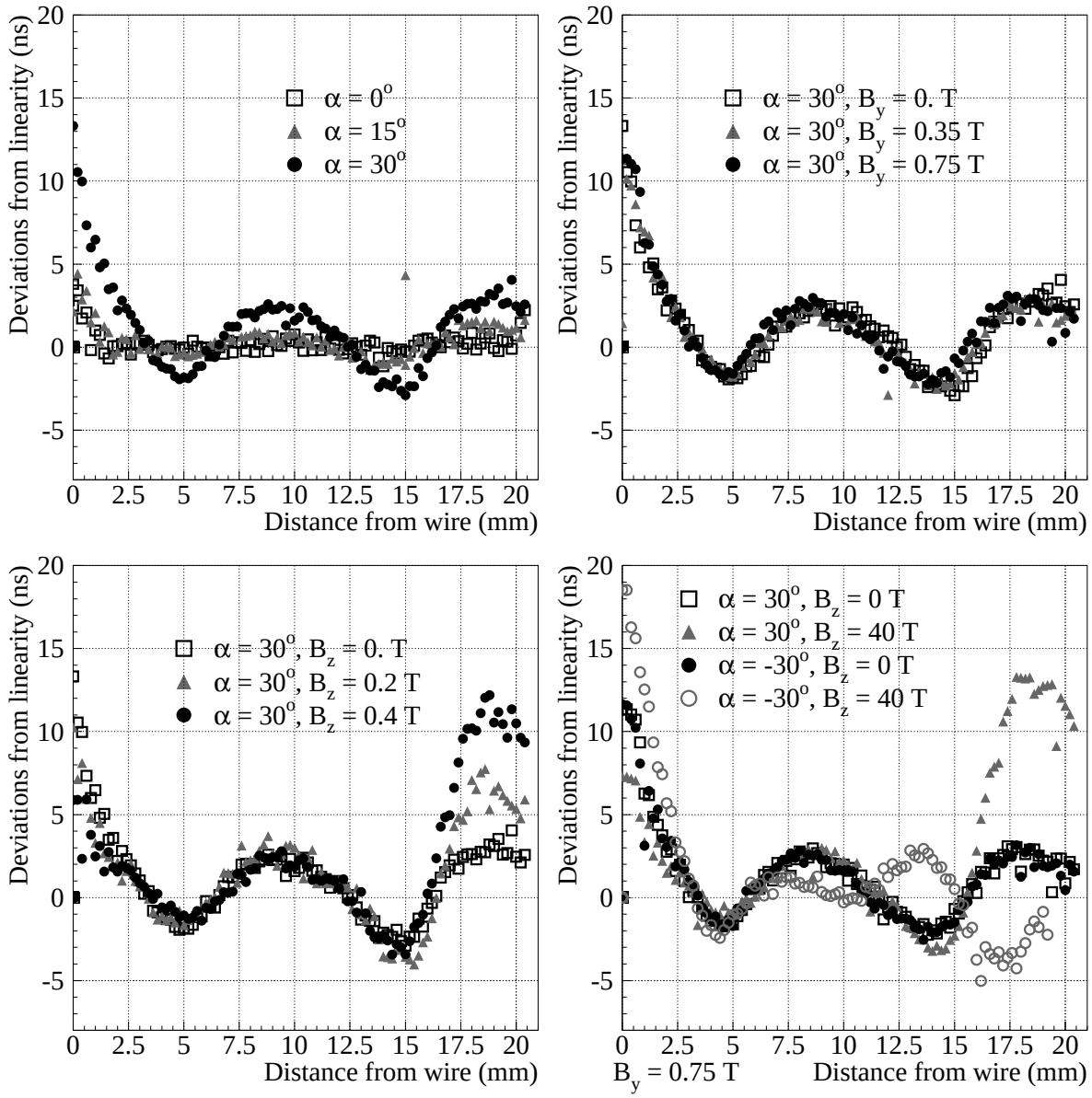

Figure 10: (Upper left) Deviations from linearity for different angles with no magnetic field, (upper right and lower left) different B_y and B_z values at 30 degrees, and (lower right) extreme cases of B_z fields at 30 degrees. The asymmetry between positive and negative angles is clearly seen in the presence of B_z.

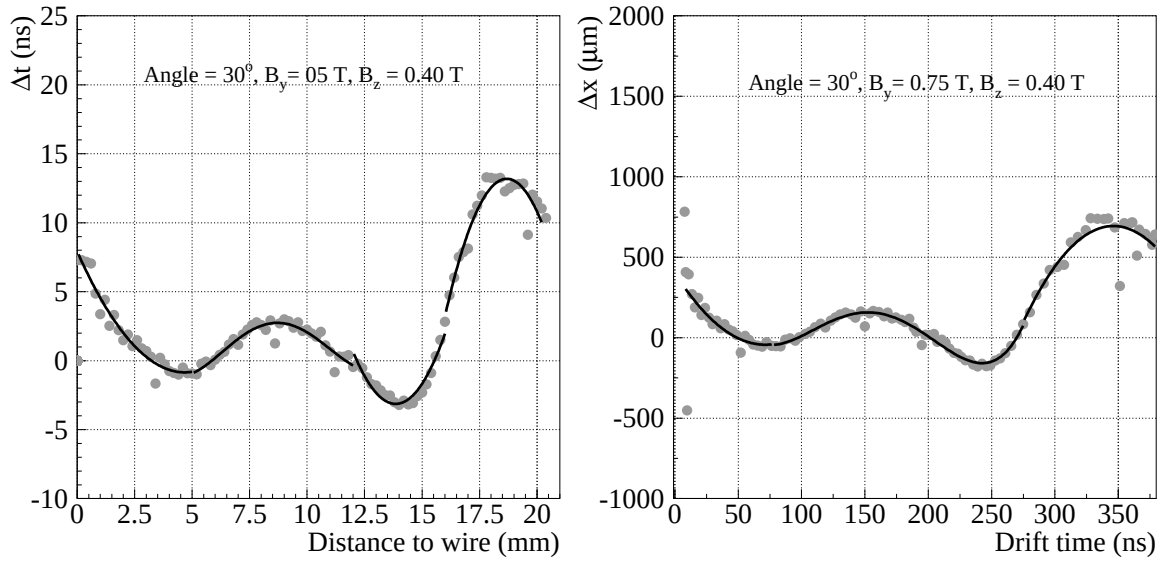

Figure 11: (Left) Deviations from linearity in time versus cell position and (right) in distance versus drift time. The dots represent the simulation, whereas the continuous lines indicate the polynomial branches used for the parametrization.

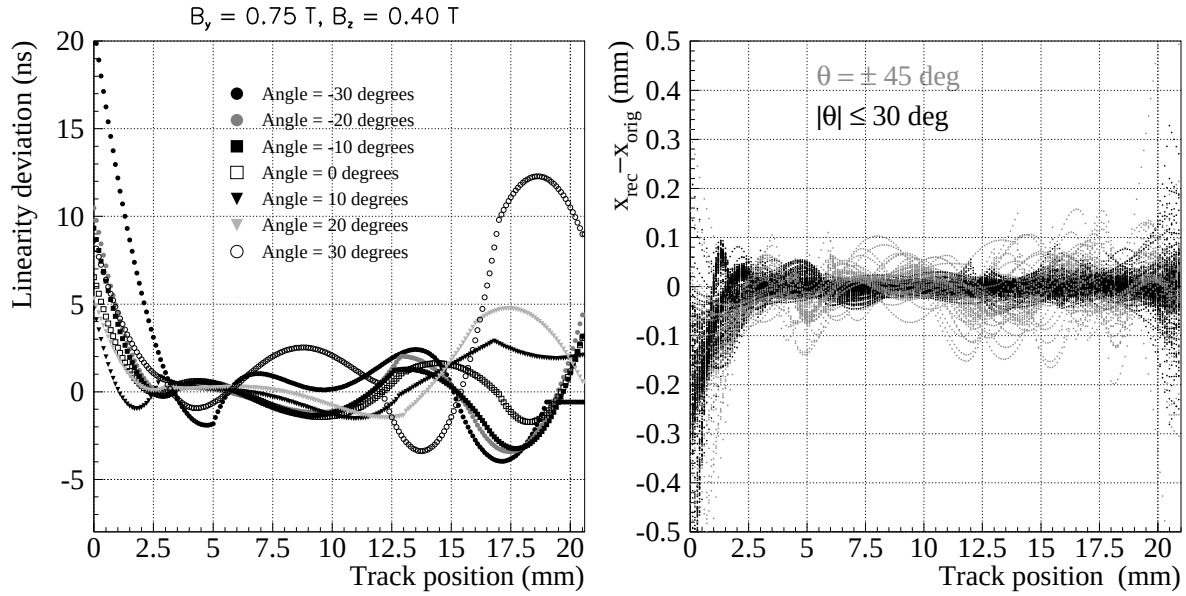

Figure 12: (Left) Δt values returned by the parametrization function for the maximum simulated B_y and B_z values. (Right) Difference between the simulated position of a particle and the position returned by first applying the parametrized function to convert position to time and then applying the function to convert time to position. All the simulated configurations are superimposed, for $|\theta| \leq 30$ degrees in black and for $\theta = \pm 45$ degrees in gray. Large deviations from zero correspond to large θ values.